Effect of polarization mimicking cathodic electrodeposition coating on industrially relevant metal substrates with ZrO_2 based conversion coatings

Adnan Sarfraz [*] Ralf Posner[†] Asif Bashir[*]
Angel Topalov[*] Karl J. J. Mayrhofer[*] Kirsten Lill[†]
Andreas Erbe [‡*§]

1 Abstract

Modern ZrO_2-based conversion coatings were deposited on an aluminium alloy (AA6014), a cold rolled steel, an zinc electrogalvanised steel, and a Sendzimir zinc hot-dip galvanised steel. Pretreated substrates were subjected to galvanostatic polarization in aqueous $NaNO_3$ to mimic deposition conditions of cathodic electrodeposition coatings. No significant structural modification of the conversion coatings was found by Raman and photoluminescence (PL) spectroscopy. After treatment, increased photoluminescence indicated an increased amount of point defects. Downstream monitoring of dissolved Zr indicated an insignificant totally dissolved fraction of $\sim$0.01% after 5 s of polarization, which may occur through vacancy pair coalescence with concurrent oxide dissolution, as discussed for transpassive dissolution. Overall, the ZrO_2 films remained intact after polarization.

2 Introduction

Conversion coatings serve the purpose of protecting the base metal from corrosion, e.g. by promoting adhesion to the further organic coating layers. Recently,

[*]Max-Planck-Institut für Eisenforschung GmbH, 40237 Düsseldorf, Germany
[†]Henkel AG & Co KGaA, 40589 Düsseldorf, Germany
[‡]corresponding author. Tel. +49 211 6792-890; Fax +49 211 6792-218, aerbe@arcor.de, a.erbe@mpie.de
[§]Presently also at: Department of Materials Science and Engineering, NTNU, Norwegian University of Science and Technology, 7491 Trondheim, Norway

ZrO_2-based based conversion coatings have been investigated extensively as potential replacements for conventional trication phosphating. Detailed studies on the deposition mechanism and corrosion protection properties of ZrO_2-based pretreatments are available [1, 2, 3, 4, 5]. The deposition mechanism involves removal of the oxide layer, followed by precipitation of zirconium oxide along with metallic components present in the solution [1, 6, 3, 4]. Inclusion of Cu^{2+} can be beneficial for a homogeneous deposition of ZrO_2 [5, 7, 6]. Resulting coatings are composed mainly of a ZrO_2 matrix with copper rich particles [8]. In such coatings, it has been shown that copper from the pretreatment bath preferentially deposits on the intermetallic particles rich in Fe and Si on AA6014 [8]. Surface element distribution also determines deposition of ZrO_2-based conversion coatings on Zn-Al-Mg surfaces of metallic coatings [9]. Larger hydroxyl fraction on the base material enhances the deposition of ZrO_2-based conversion coatings, as shown by a larger thickness on AA6014 [10], and a detailed in situ mechanistic study on zinc oxide [11]. ZrO_2 thickness increased with increase of convection [12]. Overall, convection has a strong effect on resulting morphologies [13].

Specifically on an aluminium alloy, the presence of ZrO_2-based conversion coating showed an increase in the adhesion to high molecular weight epoxy coating [14]. AFM scratch tests to study adhesion properties of epoxy, acrylic, and polyester based coatings showed significant improvement on cold rolled steel [15].

After pretreament, however, samples are frequently coated by a cathodic electrodeposition (CED) coating, e.g. for automotive applications. Deposition of the organic CED coating is typically performed by applying voltages between 150 and 200 V in a two electrode configuration, where the surface to be coated serves as cathode. Detailed studies are available in the literature on the corrosion and adhesive properties of the resulting coatings [5, 14, 16]. The degradation of phosphate and other conversion coatings due to the cathodic treatment has been discussed [17, 18]. On the other hand, studies focusing on the effect of the high applied potentials and the consequent current flow on the structure and properties of ZrO_2-based conversion coatings are not available in the literature. However, loss or damage of the coating would significantly diminish corrosion protection. One of the reasons for the absence of such data is the inaccessibility for analytical methods of the conversion coating upon deposition of the opaque thick paint layer.

Several potential mechanisms of damage to the ZrO_2-based coating can be thought of. ZrO_2 is known to be an ionic conductor [19, 20]. Transport of charges through ZrO_2 must nevertheless be accompanied by follow-up processes inside the solid. Mechanisms similar to those discussed for transpassive dissolution may occur, e.g. vacancy pair coalescence under concurrent dissolution of oxide [21]. Alternatively, the cathodic currents and the resulting hydrogen evolution may shift the pH near the surface into the alkaline, leading to dissolution of the ZrO_2 under zirconate formation [22].

This work focuses on the study of the effect of cathodic polarization at current densities as encountered in the CED process on ZrO_2-based conversion coatings. Conversion coatings were produced on well-defined standard

samples of four metal substrates commonly used in the automotive industry: aluminium alloy AA6014, an electrogalvanised steel (MBZE), a Sendzimir hot dip galvanized steel (EA) and a cold rolled steel (MBS) were used. Galvanostatic polarization was conducted in $NaNO_3$ as model electrolyte, because it suppressed strong bubble formation of hydrogen gas. During polarization, the interfaces were monitored by in situ Raman spectroscopy and in situ photoluminescence (PL) spectroscopy. Polarization was also carried out in the presence of a transparent CED binding agent. The amount of dissolved Zr was monitored downstream by inductively coupled mass spectrometry (ICP-MS) in a flow cell. Surfaces before and after polarization were compared by scanning Kelvin probe force microscopy (SKPFM) to gain insight into changes in the surface potential originating from the polarization of the surface.

3 Results and Discussion

When polarizing a metal substrate in a solution of the CED binding agent, a porous organic layer on top of the conversion coating resulted. Figure 1 shows a scanning electron microscopy (SEM) image of the porous polymer film, where the substrate is visible through the pores. The porous nature of the film facilitated measurements by Raman spectroscopy in a confocal microscope of the substrate under the polymer film.

Figure 2 shows Raman spectra of samples polarized with binding agent, and spectra of unpolarized, pretreated samples. After polarizing the samples, Raman spectra were measured by either focusing through the polymer layer using the confocal setup or by measuring in the pores present in the top layer as shown in Figure 1. The Raman spectrum of pretreated AA6014 has been discussed in detail previously [8]. The Raman spectrum of ZrO_2-pretreated cold rolled steel is almost identical to that of AA6014. In the case of the zinc electrogalvanised steel samples, peaks from the ZrO_2-based pretreatment were absent due to the lower thickness of the conversion coating on this substrate, and the dominance of the peak arising from the underlying ZnO. The observed peaks are discussed briefly below.

The major peaks observed in the spectra of cold rolled steel and AA6014 at 297 and 628 cm^{-1}, with a shoulder at 343 cm^{-1}, are characteristic for crystalline Tenorite CuO [23, 24, 25, 26]. The broad peak present at 1110 cm^{-1} is assigned as the second harmonic of the B_g mode of CuO at 628 cm^{-1}. The major component of the conversion coating ZrO_2 is exhibiting only a few weak peaks in the spectra at 233 and 470 cm^{-1}. This can be attributed to the amorphous nature of ZrO_2 present in the sample [27].

In the case of zinc electrogalvanised steel and zinc hot dip galvanised steel, three known peaks originating from ZnO were identified. The dominating broad peak has two components. The first is centred around $\sim$440 cm^{-1} and corresponds to the characteristic E_2 mode of ZnO with a hexagonal wurtzite lattice. The second peak at $\sim$570 cm^{-1} corresponds to longitudinal optical (LO) phonons (E_1 and A_1 modes) [28, 29, 30]. A low intensity peak present at around

$\sim$330 cm^{-1} is originating from a multiphonon process [31, 32]. Spectra as observed here are typical for defect-rich ZnO [30], obtained in electrochemical or corrosion processes [33, 34].

Comparing the Raman spectra recorded on pretreated cold rolled steel before and after polarization (Figure 2a) shows the disappearance of the second harmonic of the B_g mode of CuO and an increase in the luminescence peak starting from around 1000 cm^{-1} (<2.29 eV). The luminescence does not peak in the accessed spectral range, which goes down to 2.10 eV. In the case of pretreated AA6014 (Figure 2b), one major difference is the increase in luminescence upon polarization. Moreover, a new Raman peak centred around 300 cm^{-1} appeared in the Raman spectrum of the polarized sample. For both conversion film coated AA6014 and cold rolled steel, the major peaks arise from nm to μm sized copper rich particles present on the surface as discussed previously [8]. Apart from the disappearance of the second harmonic, a decrease in intensity of Raman peaks, along with slight broadening of the peaks present is observed. It has previously been shown that changes in the particle size and microstructure of copper oxide leads to broadening of the Raman peaks [35]. The observations here can be interpreted such that a decrease in the particle size of the copper oxide of the copper rich particles happened during polarization. The observed increase in background luminescence could be caused by an increasing defect density (and hence, an increased density of intra-gap states of semiconducting oxides). For electrochemically formed copper oxides, strong PL was observed previously with green excitation, which was attributed to an otherwise forbidden band-to-band transition which becomes active for defect-rich mixed oxides [36]. Luminescence may, however, also originate from intra-gap states in ZrO_2, or other metal oxides involved. Overall, however, the increase in background luminescence is a strong indicator for an increase in the density of point defects in the layers. As the peak energy wasn't determined, no statement can be made on the nature of the defects.

In the case of pretreated zinc electrogalvanised steel (Figure 2c), two differences were observed in the spectra when comparing the state before and after polarization. Firstly, the broad peak at 580 cm^{-1} increased in intensity after polarization. Secondly, the luminescence background also increased significantly. This increase is interpreted along the same line as the increase in intensity of the ZnO LO phonon as increase in amount of point defects in the oxide films.

Finally, comparing the spectra of conversion film coated zinc hot dip galvanised steel (Figure 2d), no change was observed other than a slight broadening of the peak at 580 cm^{-1}. Since non-polarized samples already exhibited a high luminescence background, it can be concluded that the density of point defects does not increase significantly upon polarization.

More insight into the nature of the changes may be obtained from in situ Raman measurements, which are so far only possible in the absence of the binding agent and where hence conducted in $NaNO_3$ as model electrolyte. In situ Raman spectra of the conversion film coated samples are shown in Figure 3. The three major Raman peaks seen in the spectra (around 1020, 1390, and 1630 cm^{-1}) all originate from the solution: the former two are assigned to nitrate

stretching modes [37], while the latter one is the water bending mode. In all the three experimental series shown, one each for cold rolled steel, AA6014 and zinc electrogalvanised steel, a cathodic current of 4 mA cm^{-2} was applied after recording the first three spectra. The most evident consequence of electrode polarization in all cases was a significant increase in the background luminescence. This matches the conclusions derived from the ex situ measurements. The observation of increased luminescence also after the polarization was switched off indicates that the increase in luminescence is not entirely due to electroluminescence, i.e. a recombination of electron-hole pairs which are generated by forcing a current flow in galvanostatic polarization, but is indeed photoluminescence.

From the Raman experiments, no evidence is found for the disintegration of the ZrO_2-based conversion coatings. Consequently, ICP-MS as a more sensitive method for detection of the dissolved amount of Zr in solution was used to measure concentrations of dissolved Zr in the electrolyte during cathodic polarization. Resulting integrated dissolution profiles for the different pretreated substrates are shown in Figure 4. For each conversion film coated substrate once a current was applied, a zirconium signal was detected. It was observed that after ≈200 s of polarization, the Zr signal disappeared. Consequently, dissolution stopped at some point even though current was still applied. This observation may indicate that only a certain fraction of the conversion coating can actually be dissolved, and the remaining coating is stable. The time traces of the Zr-signal were integrated up to two different total times. To obtain the total amount of dissolved Zr, the whole curve was integrated for 120 s of cathodic polarization, a typical time of CED coating formation. However, in the CED process, after ≈5 s, the surface is already coated and the current densities decrease significantly. Therefore, the traces of dissolved Zr were integrated also up to 5 s, which should yield a realistic estimate of the amount of dissolved Zr. Results are compiled in Table 1. The integrated dissolved masses of Zr have been normalised to the mass of the conversion coatings to obtain fractions of dissolved Zr [5]. The mass of similar coatings on different surfaces have been reported to be in the range of 2-6.5 $\mu g/cm^2$ after 120 s of coating [5]. In this work, a value of 6.5 $\mu g/cm^2$ was used for normalisation. As shown in Table 1, the fraction dissolved is insignificant, as it is less than 0.1% of the total mass. The differences observed between the different substrates may have different origins. The roughness and hence the available surface area may be slightly different. However, dissolution from the flatter aluminium alloy surface is higher than from the rough EA coating. Therefore, it is more likely that the binding of the ZrO_2-based conversion coating to the surface of the different substrates is slightly different, and these differences are responsible for the observed differences in dissolution.

SKPFM studies were performed before and after polarization to evaluate whether work function contrast on the surfaces changed for conversion coated AA6014. Morphology, Volta potential map and the distribution of the Volta potentials are shown in Figure 5. The bright spots seen in the morphology and Volta potential maps of the non-polarized sample (Figure 5a,b) agree in size to copper rich particles [8], which are cathodic in the deposition process [5], similar

to intermetallic particles in corrosion [38]. It is therefore safe to assume that the cathodic spots before polarization are indeed the copper rich particles. Comparing the morphologies of polarized and non-polarized samples (Figure 5a and d) shows no significant differences. On the other hand, the Volta potential maps (Figure 5b and e) look significantly different. The cathodic regions (higher potentials on the map) are no longer localized, but rather distributed evenly over the surface. Therefore, after polarization, the Volta potentials became more broadly distributed (Figure 5f) when compared to the sharp distribution before polarization (Figure 5c). Consequently, during polarization, a significant remodelling of the surface occurred. This remodelling may be dissolution and re-deposition of the surface atoms. It is also possible that the initially cathodic copper-rich particles become significantly altered in the polarization process. In both cases, changes happened in a region of the top few atomic layers and thus, no change in the morphology was detected, whereas changes were clearly visible in the Volta potential map. Especially for aluminium alloys, cathodic inclusions effectively accelerate filiform propagation in under-paint corrosion processes [39, 40]. While in the absence of specific cathodic "hot-spots", other regions of the surface take the role of cathodes in filiform corrosion [41], distributing cathodic regions evenly on an AA surface is expected to slow down under-paint corrosion. Because it was not possible to polish the substrates with metallic coatings, no systematic study with all substrates using SKPFM has been conducted. However, no special effect of the intermetallic inclusions in the aluminium alloys is expected on the potential distribution after polarization. Therefore, the observed potential distribution after polarization may be similar on the other substrates as well.

4 Summary and Conclusions

The main conclusion from this work is that cathodic polarization of the investigated metal substrates and metallic coatings (AA6014, cold rolled steel, zinc electrogalvanised steel, zinc hot dip galvanised steel) with ZrO_2-based conversion coatings under current densities similar to those encountered in the cathodic electrodeposition process does not lead to significant structural alterations of the conversion coatings. Surface morphology and the vibrational modes in Raman spectra remain virtually unaltered, and no indication was found of significant conversion coating loss during polarization. Detected Zr dissolution is negligible with dissolving mass fractions in the order of 0.001 or below. The fact that dissolution stopped even though current is still being applied shows that only a certain fraction of the conversion coating is prone to dissolution. The stop of the dissolution is an indication that the alkaline dissolution of the coatings is not the main mechanism of dissolution, as alkaline dissolution is not supposed to stop while a current is still being applied. After polarization, however, the distribution of cathodic regions on AA6014 on the surface has changed considerably. Furthermore, the PL background of recorded Raman spectra increased in all substrates except for zinc hot dip galvanised steel directly with the application

of the current. This observation is attributed to an increased amount of point defects in the coatings, which may well contribute to the observed remodelling of the surface, which is manifested by Volta potential differences and the contrast inversion in the SKPFM images after polarization. Coating remodelling is expected to have a positive impact on interface stability. In the available spectral range (> 2.1 eV), no clear maximum of the PL spectra was observed, which hinders a more detailed interpretation of the spectra. The forming point defects may also contribute to the dissolution. Defects may migrate to the surface and then lead to dissolution, as discussed for transpassive dissolution. Defects remaining inside the coating lead to the increase in PL. The technology applied here, i.e. an investigation by Raman spectroscopy of the region between polymer film and the metal substrate, is highly suitable for further studies of different problems of similar nature.

5 Experimental Section

In this work, samples of AA6014 (Mg ≤0.8 wt.%, Fe ≤0.35 wt.%, Si ≤0.6 wt.%, Cu ≤0.2 wt.%, Mn ≤0.2 wt.%, balance Al), an electrogalvanised steel (MBZE), a Sendzimir hot dip galvanized steel (EA; in the metallic coating 5-20 mg m^{-2} Al, balance Zn) and a cold rolled steel (MBS; C ≤0.1 wt.%, Mn ≤0.50 wt.%, P ≤0.030 wt.%, S ≤0.035 wt.%, balance Fe) were used. Samples were supplied by Henkel (Düsseldorf, Germany).

Before deposition of the ZrO_2-based conversion coatings, the sample surfaces were first immersed for 3 min in an alkaline cleaner solution at pH 10.9 at 55°C. This alkaline cleaner solution contained 3% of Ridoline 1574 and 0.3% of Ridosol 1270 (Henkel, Düsseldorf, Germany). After rinsing with deionized water, pretreatment was conducted by 120 s immersion of the substrates in a modified hexafluorozirconic acid solution (Henkel, Düsseldorf, Germany) that contained <200 mg L^{-1} Zr and <50 mg L^{-1} Cu, as used previously [8]. The pH of the solution was adjusted to 4 by using Neutralizer 700 (Henkel, Düsseldorf, Germany). All samples were rinsed with deionized water and dried in a nitrogen stream after the thin film deposition process.

Galvanostatic cathodic polarization of the pretreated samples was carried out using two different methods, (a) for in situ spectroscopy employing a model electrolyte and (b) with the binding agent of the cathodic dip coating solution. Polarization with model electrolyte was done using 0.1 M $NaNO_3$. The in situ spectroscopy setup is shown schematically in Figure 6 (see [42] for details). The model solution flows through the cell with the electrode surface area of 0.785 cm^2. The counter electrode was a graphite rode, and reference electrode was a an Ag/AgCl(3M KCl) microreference electrode. A cathodic current density of 4 mA cm^{-2} was applied for 120 s while spectra were continuously recorded.

For polarization with a binding agent, a 50% solution of the binding agent (Cathoguard, BASF Coatings, Münster, Germany) was used as electrolyte. Similar to the in situ measurements, the reference and counter electrodes were

Ag/AgCl(3M KCl) and graphite, respectively. For the cathodic dip coating of metal parts, normally a few minutes of cathodic current is applied to deposit a thick layer of the CED coating. In this work, cathodic current densities of 4 mA cm^{-2} were applied for 5 s so that the metal substrate remained partly uncovered.

Raman spectra were recorded on a Horiba Jobin Yvon Labram confocal Raman microscope with an excitation wavelength of 514 nm (2.41 eV). In the setup shown in Figure 6, the light was focused on the sample surface through a 50× long working distance objective (NA = 0.5). The setup was described in more detail elsewhere [42].

Concentrations of dissolved Zr were measured using an electrochemical flow cell connected to an inductively coupled plasma mass spectrometer (ICP-MS) Perkin Elmer NexION 300X. The cell was interfaced to a Gamry Reference 600 potentiostat; system and control software were described in detail previously [43, 44, 45]. Pretreated samples were used as working electrodes in 0.1M $NaNO_3$ electrolyte with a contact area of 1.1 mm^2. A thin graphite rod counter electrode was placed in the inlet tube and an Ag/AgCl(3M KCl) reference electrode was connected downstream. An internal standard (^{187}Re) was added downstream of the electrochemical cell to ensure a constant performance of the ICP-MS. During dissolution concentration monitoring, the samples were polarized in total for 300 s. During the initial 30 s, the cathodic current was ramped up from 0 to 4 mA cm^{-2}. Subsequently, the cathodic current was held at this value.

The SKPFM measurements were carried out on an Agilent 5500 SPM. The operational and instrumental details of the instrument equipped with an environmental chamber have been described elsewhere [46]. The atomic force microscope tips made of silicon were coated with Pt/Ti (20 nm) on the top side and an Al reflex coating at the back side. Tip radius was 28±10 nm at the apex. Two different sets of measurements were carried out, one before and one after polarization. A prerequisite of SKPFM measurements is a polished substrate, thus only selected substrates could be measured using this technique.

Scanning electron microscopy (SEM) was performed with a Zeiss Leo 1550VP Gemini (Carl Zeiss SMT AG, Germany). Images were obtained in secondary electron contrast with an acceleration voltage of 5-10 kV and a working distance of 5-7 mm.

6 Acknowledgement

A.S. and A.E. acknowledge Henkel AG & Co. KGaA, Düsseldorf, for funding a collaborative research project. Prof. M. Stratmann is acknowledged for his continuous support. The MPIE machine shop is acknowledged for building the in situ cell.

7 Keywords

aluminium alloy, cathodic electrodeposition, conversion coatings, galvanised steel, point defects

8 TOC

ZrO_2-based conversion coatings on structural materials (see picture) remain intact after cathodic polarization. Consequently, they survive the application of cathodic electrodeposition coating, a process frequently used e.g. in the automotive industry. Some surface remodelling takes place during polarization. In situ and ex situ spectroscopy show increased defect-related luminescence.

References

[1] M. Rohwerder, M. Stratmann, G. Grundmeier, *Corrosion Mechanisms in Theory and Practice* (Ed.: P. Marcus), CRC Press, Boca Raton, FL, USA **2012**. pp. 617–667.

[2] R. Twite, G. Bierwagen, *Prog. Org. Coat.* **1998**, *33*, 91.

[3] P. Taheri, K. Lill, J. de Wit, J. Mol, H. Terryn, *J. Phys. Chem. C* **2012**, *116*, 8426.

[4] S. Wang, L. Wang, C. Liu, *Acta Metall. Sin.* **2011**, *24*, 18.

[5] S. Adhikari, K. A. Unocic, Y. Zhai, G. S. Frankel, J. Zimmerman, W. Fristad, *Electrochim. Acta* **2011**, *56*, 1912.

[6] J. Cerezo, I. Vandendael, R. Posner, K. Lill, J. H. W. de Wit, J. M. C. Mol, H. Terryn, *Surf. Coat. Technol.* **2013**, *236*, 284.

[7] T. Lostak, S. Krebs, A. Maljusch, T. Gothe, M. Giza, M. Kimpel, J. Flock, S. Schulz, *Electrochim. Acta* **2013**, *112*, 14.

[8] A. Sarfraz, R. Posner, M. M. Lange, K. Lill, A. Erbe, *J. Electrochem. Soc.* **2014**, *161*, C509.

[9] T. Lostak, A. Maljusch, B. Klink, S. Krebs, M. Kimpel, J. Flock, S. Schulz, W. Schuhmann, *Electrochim. Acta* **2014**, *137*, 65.

[10] J. Cerezo, P. Taheri, I. Vandendael, R. Posner, K. Lill, J. de Wit, J. Mol, H. Terryn, *Surf. Coat. Technol.* **2014**, *254*, 277.

[11] P. Taheri, P. Laha, H. Terryn, J. Mol, *Appl. Surf. Sci.* **2015**, *356*, 837.

[12] J. Cerezo, R. Posner, I. Vandendael, J. H. W. de Wit, H. Terryn, J. M. C. Mol, *Mater. Corros.* **2015**, *67*, 361.

[13] O. Lunder, C. Simensen, Y. Yu, K. Nisancioglu, *Surf. Coat. Technol.* **2004**, *184*, 278.

[14] N. Khun, G. Frankel, J. Zimmerman, *Corrosion* **2012**, *69*, 259.

[15] S. Adhikari, G. S. Frankel, B. D. Bammel, J. Zimmerman, *J. Adhes. Sci. Technol.* **2012**, *26*, 1591.

[16] H. Eivaz Mohammadloo, A. A. Sarabi, R. Mohammad Hosseini, M. Sarayloo, H. Sameie, R. Salimi, *Prog. Org. Coat.* **2014**, *77*, 322.

[17] L. Jiang, M. Wolpers, P. Volovitch, K. Ogle, *Corros. Sci.* **2012**, *55*, 76.

[18] L. Jiang, M. Wolpers, P. Volovitch, K. Ogle, *Surf. Coat. Technol.* **2012**, *206*, 3151.

[19] M. Aoki, Y.-M. Chiang, I. Kosacki, L.J.-R. Lee, H. Tuller, Y. Liu, *J. Am. Ceram. Soc.* **1996**, *79*, 1169.

[20] T.H. Etsell, S.N. Flengas, *Chem. Rev.* **1970**, *70*, 339.

[21] D.D. Macdonald, *J. Electrochem. Soc.* **1992**, *139*, 3434.

[22] M. Maraghini, E. Deltombe, N. de Zoubov, P. Van Rysselberghe, M. Pourbaix, Zirconium. (Ed.: M. Pourbaix), National Association of Corrosion Engineers / CEBELCOR, Houston / Brussels, 1974, pp. 223-229.

[23] J. Chrzanowski, J. Irwin, *Solid State Commun.* **1989**, *70*, 11.

[24] H. F. Goldstein, D.-s. Kim, P. Y. Yu, L. C. Bourne, J.-P. Chaminade, L. Nganga, *Phys. Rev. B* **1990**, *41*, 7192.

[25] S. N. Narang, V. B. Kartha, N. D. Patel, *Phys. C (Amsterdam, Neth.)* **1992**, *204*, 8.

[26] L. Debbichi, M. C. Marco de Lucas, J. F. Pierson, P. Krüger, *J. Phys. Chem. C* **2012**, *116*, 10232.

[27] V. G. Keramidas, W. B. White, *J. Am. Ceram. Soc.* **1974**, *57*, 22.

[28] T. C. Damen, S. P. S. Porto, B. Tell, *Phys. Rev.* **1966**, *142*, 570.

[29] C. A. Arguello, D. L. Rousseau, S. P. S. Porto, *Phys. Rev.* **1969**, *181*, 1351.

[30] Y. Y. Tay, T. T. Tan, M. H. Liang, F. Boey, S. Li, *Appl. Phys. Lett.* **2008**, *93*, 111903.

[31] J. M. Calleja, M. Cardona, *Phys. Review B* **1977**, *16*, 3753.

[32] Ü. Özgür, Y. I. Alivov, C. Liu, A. Teke, M. A. Reshchikov, S. Dogan, V. Avrutin, S. J. Cho, H. Morkoç, *J. Appl. Phys.* **2005**, *98*, 041301.

[33] Y. Chen, P. Schneider, B.-J. Liu, S. Borodin, B. Ren, A. Erbe, *Phys. Chem. Chem. Phys.* **2013**, *15*, 9812.

[34] D. Iqbal, A. Kostka, A. Bashir, A. Sarfraz, Y. Chen, A. D. Wieck, A. Erbe, *ACS Appl. Mater. Interfaces* **2014**, *6*, 18728.

[35] J. F. Xu, W. Ji, Z. X. Shen, W. S. Li, S. H. Tang, X. R. Ye, D. Z. Jia, X. Q. Xin, *J. Raman Spectrosc.* **1999**, *30*, 413.

[36] C. Toparli, A. Sarfraz, A. Erbe, *Phys. Chem. Chem. Phys.* **2015**, *17*, 31670.

[37] I. Nakagawa, J. L. Walter, *J. Chem. Phys.* **1969**, *51*, 1389.

[38] F. Andreatta, A. Turco, I. de Graeve, H. Terryn, J. de Wit, L. Fedrizzi, *Surf. Coat. Technol.* **2007**, *201*, 7668.

[39] C. Senöz, M. Rohwerder, *Electrochim. Acta* **2011**, *56*, 9588.

[40] C. Senöz, S. Borodin, M. Stratmann, M. Rohwerder, *Corros. Sci.* **2012**, *58*, 307.

[41] O. Lunder, K. F. Heen, K. Nisancioglu. *Corrosion (Houston, TX, U. S.)* **2004**, *60*, 622.

[42] G. Genchev, A. Erbe, *J. Electrochem. Soc.* **2016**, *163*, C333.

[43] A. A. Topalov, A. R. Zeradjanin, S. Cherevko, K. J. J. Mayrhofer, *Electrochem. Commun.* **2014**, *40*, 49.

[44] S. O. Klemm, A. A. Topalov, C. A. Laska, K. J. J. Mayrhofer, *Electrochem. Commun.* **2011**, *13*, 1533.

[45] A. A. Topalov, I. Katsounaros, J. C. Meier, S. O. Klemm, K. J. J. Mayrhofer, *Rev. Sci. Instrum.* **2011**, *82*, 114103.

[46] S. Magonov, J. Alexander, *Advanced Atomic Force Microscopy: Probing Electrostatic Force Interactions*. Agilent Technologies, Chandler, AZ, USA **2008**.

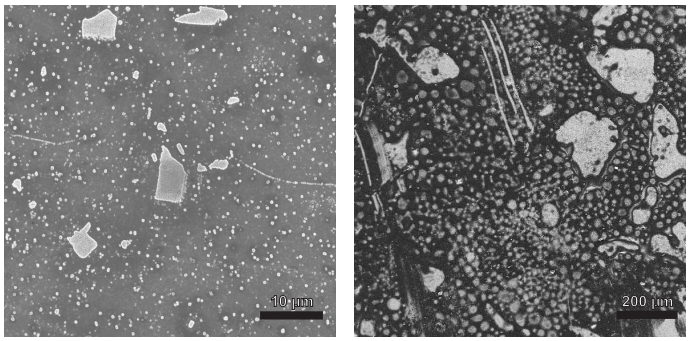

Figure 1: SEM images at two different magnifications of a AA6014 sample with ZrO_2-based conversion coating after being polarized for 5 s in a 50% CED binding agent solution. A discussion of the images of pretreated AA6014 is available elsewhere [8].

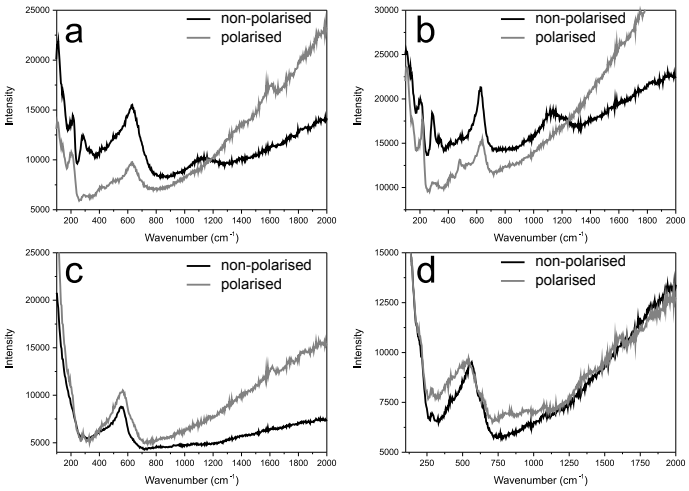

Figure 2: Ex situ Raman spectra of ZrO_2-pretreated non-polarized and polarized samples. a) cold rolled steel, b) AA6014, c) zinc electrogalvanised steel, and d) zinc hot dip galvanised steel.

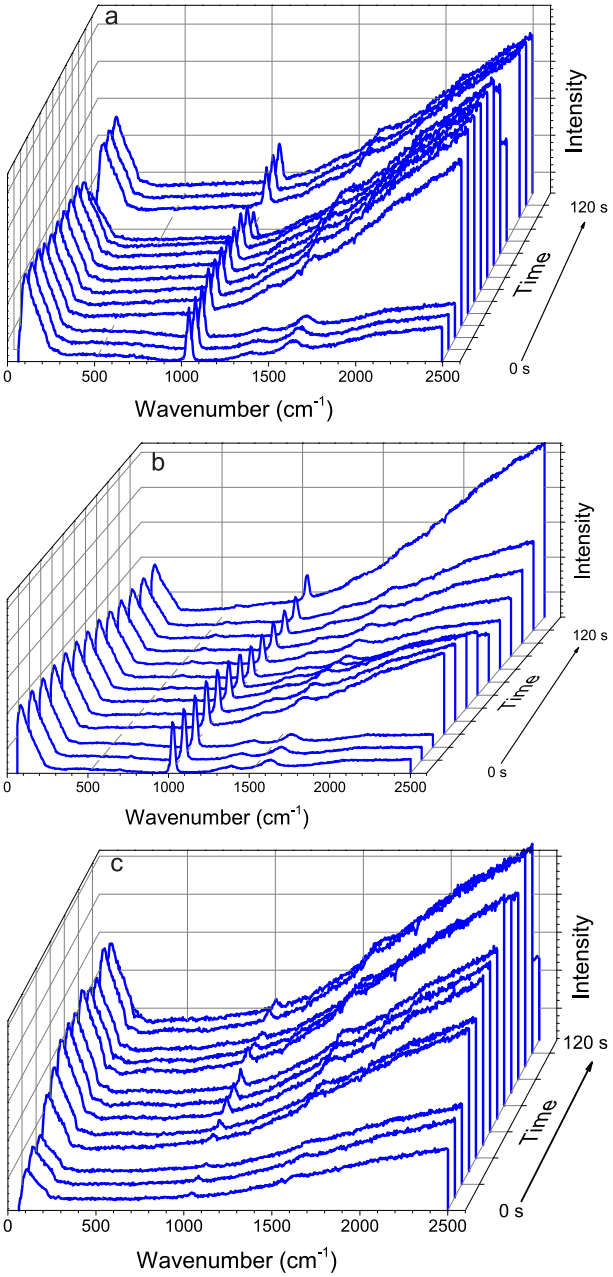

Figure 3: In situ Raman spectra of conversion film coated samples during galvanostatic polarization with a cathodic current of 4 mA cm^{-2}. a) cold rolled steel, b) AA6014, and c) zinc electrogalvanised steel

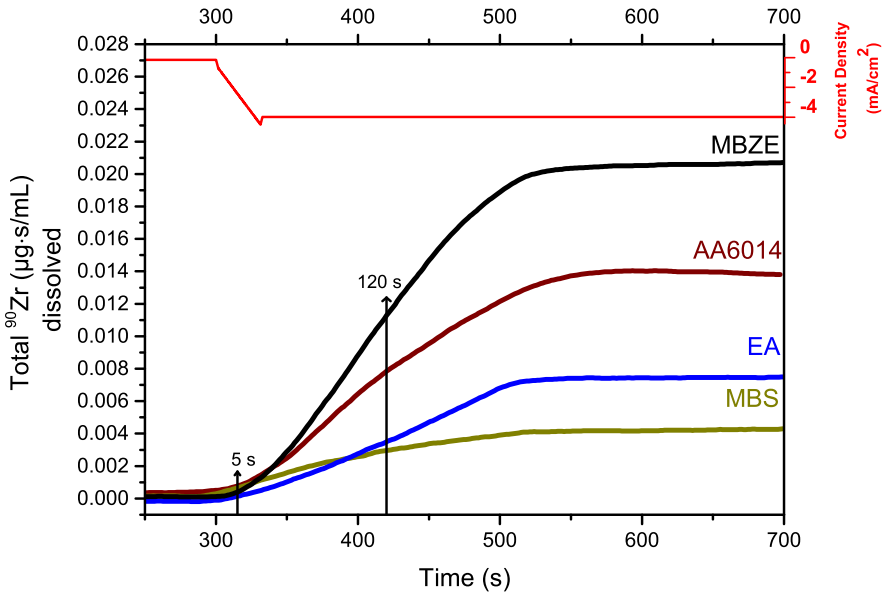

Figure 4: Integrated ICP-MS detected dissolution profiles for a total of 300 s galvanostatic cathodic polarization of four different pretreated substrates used in this work [cold rolled steel (MBS), zinc electrogalvanised steel (MBZE), zinc hot dip galvanised steel (EA), and AA6014]. A ramp from 0 to -4 mA cm^{-2} was applied for the initial 30 s. Subsequently, the current density was held at -4 mA cm^{-2}. Quantification of dissolution is shown in Table 1.

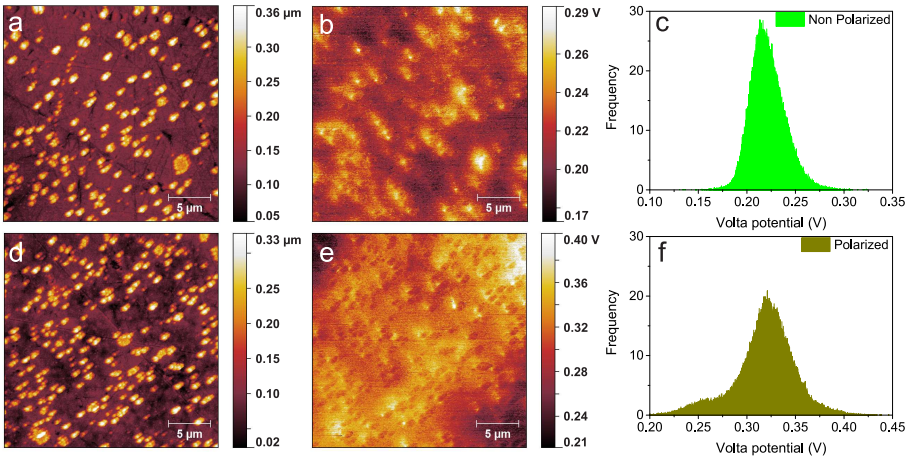

Figure 5: Morphology (a, d), Volta potential map (b, e) and the distribution of the Volta potentials (c, f) obtained from SKPFM of non-polarized (a-c) and polarized (d-f) conversion film coated AA6014.

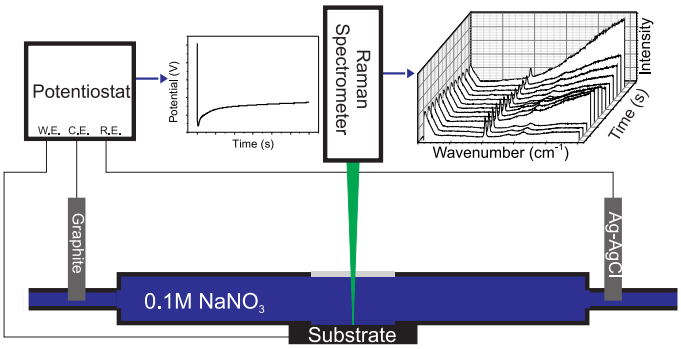

Figure 6: Schematic representation of the in situ cell used to couple the polarization experiments with Raman and PL spectroscopy.

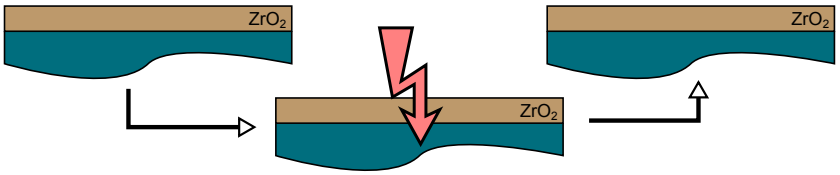

Substrate	$m_{\mathrm{diss}}^{(\mathrm{Zr})}$ (5 s) ng cm^{-2}	w_{diss} (5 s)	$m_{\mathrm{diss}}^{(\mathrm{Zr})}$ (120 s) ng cm^{-2}	w_{diss} (120 s)
Zinc electrogalvanised steel	0.25	0.00013	3.0	0.0015
AA6014	0.21	0.00011	2.5	0.0012
Cold rolled steel	0.07	0.00004	0.8	0.0004
zinc hot dip galvanised steel	0.07	0.00004	0.8	0.0004

Table 1: Integrated mass densities $m_{\mathrm{diss}}^{(\mathrm{Zr})}$ of dissolved Zr detected by downstream ICP-MS analysis after 5 s and 120 s of cathodic polarization with 4 mA cm^{-2} of different substrates with ZrO_2-based conversion coatings. Dissolved masses have been normalised to the total mass densities $m_{\mathrm{tot}}^{(\mathrm{Zr})} = 6.5\ \mu\mathrm{g/cm}^2$ of conversion coatings prepared under same conditions [5] to obtain a dissolved mass fraction w_{diss} as $w_{\mathrm{diss}} = m_{\mathrm{diss}}^{(\mathrm{Zr})}/m_{\mathrm{tot}}^{(\mathrm{Zr})}$.